

Ground-state magnetic structure of CeRh_2Si_2 and the response to hydrostatic pressure as studied by neutron diffraction

Shuzo Kawarazaki, Masugu Sato, Yoshihito Miyako, Nobusato Chigusa, and Kenji Watanabe
Graduate School of Science, Osaka University, Toyonaka, Osaka 560, Japan

Naoto Metoki and Yoshihiro Koike
Advanced Science Research Center, Japan Atomic Energy Research Institute, 2-4, Tokai, Ibaraki 319-11, Japan

Masakazu Nishi
Institute for Solid State Physics, University of Tokyo, Roppongi, Minato-ku, Tokyo, Japan
 (Received 10 May 1999; revised manuscript received 20 September 1999)

Neutron-diffraction experiments under high pressure have been done to study the magnetic structure of the ground state and the nature of the magnetic order of the pressure-induced superconductor CeRh_2Si_2 . Two models for the magnetic structure of the ground state, namely, a $4\text{-}\mathbf{q}$ superposed structure and a multidomain structure, have been tested and the former was found to be more realistic, though both of them have some inconsistency with the results of the previous NMR experiment. The pressure dependence of both the transition temperature and magnitude of the ordered magnetic moment indicate that the magnetism of this compound is basically itinerant despite its high transition temperature. Our studies also revealed that, when the pressure is close to the critical magnitude to destroy the antiferromagnetism, the compound can have a ‘‘tiny ordered moment’’ which is widely observed in the metallic Kondo-lattice compounds.

I. INTRODUCTION

The compound CeRh_2Si_2 , which has a body-centered-tetragonal structure of the ThCr_2Si_2 -type (space group $I4/mmm$), is an antiferromagnet with two transitions at 36 K (T_{N1}) and 25 K (T_{N2}).¹⁻⁴ Hydrostatic pressure of about 1 GPa destroys this antiferromagnetism and produces superconductivity below 0.4 K.^{5,6} However, this superconductivity shows a strong sample dependence: Until now, superconductivity is observed only in polycrystalline sample, and hence it is important to examine a single-crystalline sample by means of microscopic observation to study what happens in the f -electron system around the critical pressure.

On the other hand, the nature of the antiferromagnetism of this compound is also of interest: Grier *et al.*¹ have studied the magnetic structure by means of a powder neutron diffraction and determined the magnetic modulation vectors of the two antiferromagnetic phases. They also discovered characteristic behaviors in the temperature dependences of the intensities of the Bragg reflections from the two phases: At T_{N1} the Bragg reflection which represents the magnetic modulation with the wave vector of $\mathbf{q}_1 = (0.5\ 0.5\ 0)$, in the reciprocal-lattice units, appears to grow, with decreasing temperature, until the second Bragg reflection due to the magnetic modulation with $\mathbf{q}_2 = (0.5\ 0.5\ 0.5)$ starts growing at T_{N2} . The special feature in these transitions is that, in contrast with ordinary two-step phase transitions, below T_{N2} the \mathbf{q}_1 reflection is not replaced completely by the \mathbf{q}_2 reflection but both reflections remain, at low temperature, with comparable intensities. This behavior of the two intensities was qualitatively confirmed by neutron-diffraction experiments with single-crystalline specimens.² In such a situation, where one observes more than one independent reflections simulta-

neously, one has to consider two possibilities to construct the model of the magnetic structure: The reflections may represent either modulations that resides in its own magnetic domain, known as the multidomain state, or a linear combination of modulations that form a single homogeneous magnetic structure over the crystal (multi- \mathbf{q} state).⁷ The neutron-diffraction method by itself is not able to distinguish between these two states unless any special conditions or information, for instance, the theoretically allowed size of the atomic magnetic moment, are given to restrict the number of the possible structures. Discussions given in the previous studies were made mostly on the basis of the magnitude of the moment and only a $2\text{-}\mathbf{q}$ structure was considered as the possible multi- \mathbf{q} structure.^{1,2} Moreover, there is another problem as for the magnetic structure of this compound: The previous neutron-diffraction studies have reported the magnitude of the atomic magnetic moment of cerium in the ordered state to be between $1.7\mu_B$ and $2.4\mu_B$.^{1,2} Although the reported values are different from each other depending on the adopted model of the magnetic structure, none of them is less than, say, $1.5\mu_B$. On the other hand, the recent NMR study⁸ has predicted that the magnitude of the cerium moment is as small as $\sim 0.3\mu_B$ in a significant disagreement with the neutron-diffraction results. A discussion is given that this discrepancy may be caused by the difference in the characteristic time of observation between the NMR and the neutron diffraction.⁸ It is, hence, imperative to establish the ground-state magnetic structure and the size of the atomic magnetic moment of this compound.

One of the central issues of the heavy-fermion physics is of the origin of the ‘‘tiny moment order’’ which has been rather commonly observed in several paramagnetic metallic

Kondo-lattice materials: The compounds such as UPt_3 ,⁹ URu_2Si_2 ,¹⁰ CeRu_2Si_2 ,¹¹ etc., order magnetically at typically a few Kelvin with an ordered moment of 10^{-2} – $10^{-3}\mu_B/\text{Ce,U}$, though they otherwise behave as a paramagnetic Fermi-liquid material. The ‘‘paramagnetism’’ of these compounds are believed to be closely neighboring to an ordered state with a normal size of the ordered moment. Therefore, it is of importance to examine, from this point of view, the detail of the magnetic order near the critical pressure.

In the present work, we performed, in order to collect more data to determine the true magnetic structure of this compound and to consider the nature of the long-range order on the Kondo lattice, neutron-diffraction experiments by using both a single-crystalline sample and a powder sample and also by applying hydrostatic pressure. We analyzed the results in conjunction with the results of the NMR experiments while taking more model structures into considerations.

II. EXPERIMENTALS

We have made the sample crystals from stoichiometric amounts of the constituent elements with 3-N purity by first melting them in an argon-arc furnace to obtain ingots of the compound. Then we prepared the specimen for the powder-diffraction experiment by pulverizing an ingot to fine particles with sizes between 50 and 100 μm . Because the crystal of the compound CeRh_2Si_2 has very strong cleavage, the powder specimen is subject to a fateful preferred-orientation effect. In order to overcome this problem, we tried to mix the powder of the sample with about the same volume of powder of molybdenum the particle size of which is much smaller ($\sim 5\ \mu\text{m}$) than that of the sample. We expected that the molybdenum particles which fill the space around the sample particles would prevent the rotational movement of them toward the preferred orientation. In the present work, we found that this procedure works quite effectively and could reduce the resulting preferred-orientation effect small enough to be involved in the ordinary intensity analysis. The mixture was packed in a holder made of aluminum with a thin slab-shaped sample space.

We grew a single crystal of the compound from the melt of an ingot by using a three-arc furnace. The size of the crystal is $1.5 \times 1.5 \times 5\ \text{mm}^3$ and its mosaic spread is 0.6° .

The neutron-diffraction experiments have been made on the TAS-1 and the GPTAS spectrometers at the JRR-3 reactor in JAERI, Tokai, Japan. We pressurized the single-crystalline sample with a piston-cylinder-type pressure cell¹² up to 1.25 GPa at temperatures above 1.5 K.

It has been experimentally proven that the polarization of the magnetic moment of the cerium atoms in the ordered state of CeRh_2Si_2 is along the crystal c axis.^{1,2} Then the integrated intensity of the magnetic Bragg scattering is theoretically represented by the equation,

$$I(\boldsymbol{\kappa}) = B(V_D/V_0)\mu^2 \sin^2 \theta F^2(\boldsymbol{\kappa})R(\boldsymbol{\kappa}), \quad (1)$$

where B is a spectrometer-defined constant and V_D , V_0 , μ , and θ are, respectively, the volume of the domain, the volume of the sample, the size of the atomic magnetic moment and the angle between the crystal c axis and the scattering vector $\boldsymbol{\kappa}$. $F(\boldsymbol{\kappa})$ is the structure factor and $R(\boldsymbol{\kappa})$ involves all

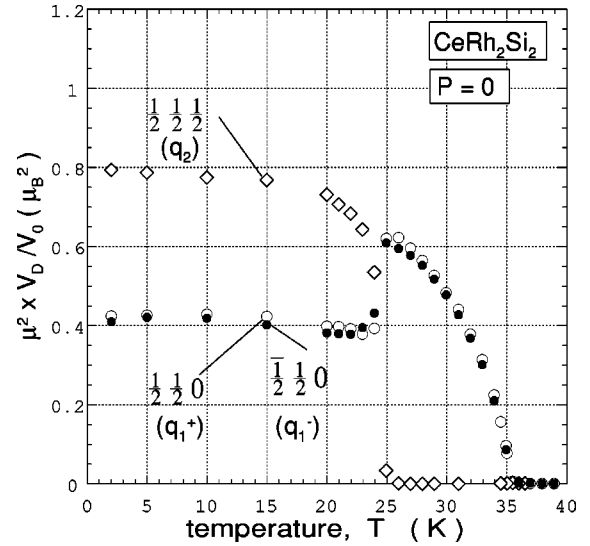


FIG. 1. The temperature dependences of the intensities of the three magnetic Bragg reflections from the single-crystalline CeRh_2Si_2 under ambient pressure. The intensities have been corrected so that they represent the product of the relative domain volume, V_D/V_0 , and the square of the atomic magnetic moment.

other $\boldsymbol{\kappa}$ -dependent factors, that is, the Lorentz factor and the absorption factor and also the preferred orientation factor and the multiplicity of the reflection for the powder experiment. The absorption factor for the powder sample was determined directly by measuring the transmission of the neutron beam. As for the form factor, the results of calculations by Lander and Brun¹³ and Freeman and Desclaux¹⁴ have been used. To put the observed intensity on an absolute basis we measured the scattering intensity of the (1 1 0) nuclear Bragg reflection as a reference. Because this reflection is so weak and has similar intensity as the magnetic reflections, we safely neglected the secondary extinction effect for this reflection.

In the present system, all the magnetic reflections reside on the reciprocal $[0.5\ 0.5\ K]^*$ axis with $K=0$, $K=0.5$, and $K=1$ and on the positions which are equivalent to them. We, therefore, took the reciprocal $[1\ 1\ 0]^*-[0\ 0\ 1]^*$ plane as the scattering plane for the measurements with the single-crystalline sample.

III. RESULTS AND DISCUSSIONS

A. The ground-state magnetic structure

In Fig. 1 shown are the plots of the intensities of the reflections from the single-crystalline sample at $K=0$, $K=0.5$, and $K=1$ as functions of temperature. In the figure, the intensities have been corrected by the known factors, $\sin^2 \theta F^2(\boldsymbol{\kappa})R(\boldsymbol{\kappa})$, and put on the absolute scale so that they represent just the product $(V_D/V_0)\mu^2$, and one can see that the intensity ratio of the reflections at $K=0$, $K=1$, and $K=0.5$ at the lowest temperature is 1:1:2 within the experimental error. Since $(0.5\ 0.5\ 1) = (101) + (-0.5\ 0.5\ 0)$, the positions $K=0$ and $K=1$ represent the wave vectors $\mathbf{q}_1^+ = (0.5\ 0.5\ 0)$ and $\mathbf{q}_1^- = (-0.5\ 0.5\ 0)$, respectively. It should be noted that the star of \mathbf{q}_1 consists of \mathbf{q}_1^+ and \mathbf{q}_1^- (Ref. 15) in the present space group of the crystal. In Fig. 2, one can see that \mathbf{q}_1^- is perpendicular to the scattering plane while \mathbf{q}_1^+ is

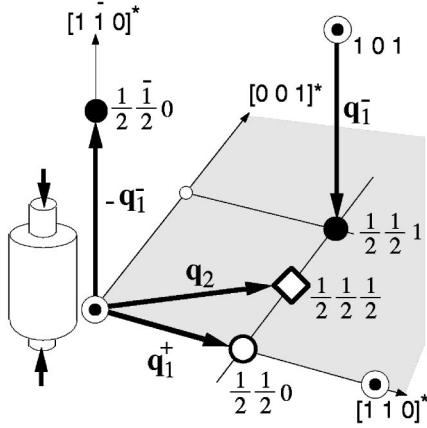


FIG. 2. The framework of the scattering space. The scattering plane is the horizontal $[110]^*-[001]^*$ plane. The $(0.5\ 0.5\ 1)$ vector is equivalent to the $(-0.5\ 0.5\ 0)$ vector which is vertical and parallel to the axis of the piston-cylinder pressure cell.

parallel to it. On the other hand, one needs some consideration as for the modulation $\mathbf{q}_2 = (0.5\ 0.5\ 0.5)$: The star of this wave vector consists of itself and its conjugate $-\mathbf{q}_2$. To see this, one should notice that, for instance, $(-0.5\ 0.5\ 0.5) = -(0.5\ 0.5\ 0.5) + (0\ 1\ 1)$. However, it is required that, in order for any modulation, except for the case of the screw structure, with a wave vector \mathbf{q} to be static and real in a crystal, it has to couple to the conjugate modulation with $-\mathbf{q}$ in the same weights. One, therefore, can regard that the modulation represented by the wave vector \mathbf{q}_2 is already in a coupled state, that is, in a $2\text{-}\mathbf{q}$ state. In Fig. 3 are shown the configurations of the magnetic moments represented by the \mathbf{q}_1^+ and the \mathbf{q}_2 modulations. Note that each configuration, $\boldsymbol{\mu}_i(\mathbf{r}_j)$, in the figure is expressed as

$$\boldsymbol{\mu}_i(\mathbf{r}_j) = A_i \exp(i\mathbf{q}_i \cdot \mathbf{r}_j + \phi_i) + \text{c.c.} \quad (2)$$

with $\phi_1 = 0$, $\phi_2 = \pi/4$ and A_i being the amplitude of the modulation and that, with this choice of ϕ_1 and ϕ_2 , $\boldsymbol{\mu}_i$ does not depend on the atomic position \mathbf{r}_j . In Fig. 1, one can see

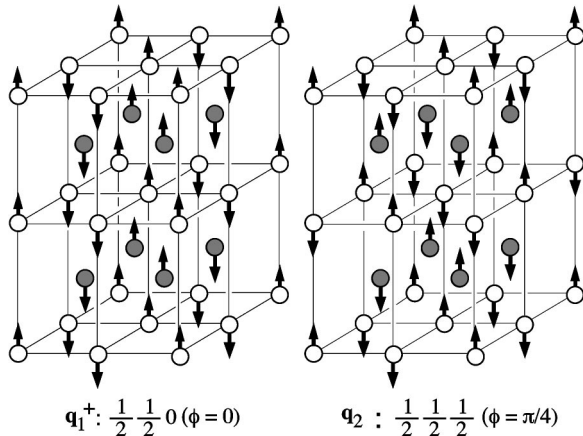


FIG. 3. The spin structures represented by Eq. (2) with $\phi_1 = 0$ for $\mathbf{q}_1^+ = (0.5\ 0.5\ 0)$ and $\phi_2 = \pi/4$ for $\mathbf{q}_2 = (0.5\ 0.5\ 0.5)$. The structure for $\mathbf{q}_1^- = (-0.5\ 0.5\ 0)$ is obtained by turning over the spins of all the body-center sites of the \mathbf{q}_1^+ structure.

TABLE I. The partial atomic magnetic moments at 4.2 K which are calculated under an assumption that all of the three modulations, \mathbf{q}_1^+ , \mathbf{q}_1^- , and \mathbf{q}_2 with $\phi_1 = 0$ and $\phi_2 = \pi/4$, share the whole crystal volume.

	$\mu_1^+(\mu_B)$	$\mu_1^-(\mu_B)$	$\mu_2(\mu_B)$
Powder sample	0.71	0.71	0.95
Single-crystalline sample	0.61	0.62	0.85

that the intensities of the \mathbf{q}_1^+ and the \mathbf{q}_1^- reflections in the temperature region $T_{N1} > T > T_{N2}$ coincide within the experimental error.

The overall features of the \mathbf{q}_1 and the \mathbf{q}_2 reflections below T_{N1} are in good agreements with the previous results. From these intensity data, one can calculate the magnitudes of the ‘‘partial’’ atomic magnetic moments μ_1^+ , μ_1^- , and μ_2 in Eq. (2) in the ground state if one assumes that each modulation occupies all the volume of the crystal, that is, $V_D = V_0$ in Eq. (1). From the data of the powder-sample diffraction one also can deduce the same information if one assumes, as ordinarily does, that the \mathbf{q}_1^+ and the \mathbf{q}_1^- modulations have the same amplitudes. In Table I shown are thus calculated values of the partial atomic magnetic moments.

The agreement between the results for the powder sample and for the single-crystalline sample is satisfactory. It is usually the case, as far as the calculation of the magnetic moment concerns, that the powder-sample diffraction has an advantage over the single-crystalline-sample diffraction: The former is free from the secondary extinction effect, from the multiple scattering effect and also from the error in the alignment of the crystal. Hereafter, we therefore, use the values obtained from the powder-sample result. Since we have three partial atomic magnetic moments (actually, we have four, μ_1^+ , μ_1^- , and the coupled two μ_2 , but we count them as three for convenience), the total atomic moment in a domain is written as

$$\boldsymbol{\mu}(\mathbf{r}_j) = \sum_i a_i \boldsymbol{\mu}_i(\mathbf{r}_j) + \text{c.c.}, \quad (3)$$

where a_i is 1 or 0 depending on whether the partial moment $\boldsymbol{\mu}_i$ is involved or not. The combination of a_i , ϕ_i and the relative volume of the domain, V_i/V_0 , V_i being the volume which the modulation \mathbf{q}_i occupies, makes a large variety of the ground magnetic structures to be chosen. Among them, we test here the following four cases as the candidates of the true ground structure.

Case (1) The \mathbf{q}_1^+ , \mathbf{q}_1^- , and the coupled \mathbf{q}_2 modulations form a $4\text{-}\mathbf{q}$ structure.

Case (2) The \mathbf{q}_1^+ and \mathbf{q}_1^- modulations form a $2\text{-}\mathbf{q}$ structure in a domain and the \mathbf{q}_2 modulation occupies another domain.

Case (3) The \mathbf{q}_1^+ and \mathbf{q}_2 modulations form a $3\text{-}\mathbf{q}$ phase in a domain and the \mathbf{q}_1^- and the \mathbf{q}_2 modulations form another $3\text{-}\mathbf{q}$ phase in another domain.

Case (4) The \mathbf{q}_1^+ , \mathbf{q}_1^- , and \mathbf{q}_2 phases reside independently in different domains.

When one tries to judge which one of these cases is real, the results of the NMR experiments by Kawasaki *et al.*⁸ are

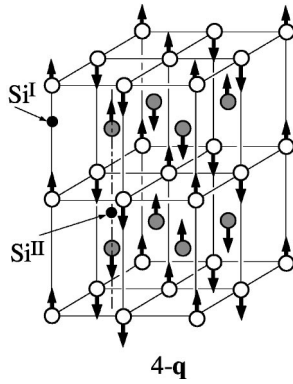


FIG. 4. The spin configuration of the 4- \mathbf{q} structure of CeRh_2Si_2 . The two silicon sites, Si^{I} and Si^{II} , are not equivalent to each other if the spin configurations of the first and the second neighboring cerium atoms along the c axis are taken into account.

useful: They measured the spin-echo spectra of ^{29}Si in CeRh_2Si_2 and CePd_2Si_2 as functions of temperature and the results for CeRh_2Si_2 are summarized as follows.

(a) At temperatures between $T_{\text{N}2}$ and $T_{\text{N}1}$, the spin-echo spectra indicate that the size of the magnetic moment of the cerium atoms is unique. There is no signal corresponding to null magnetic moment.

(b) Below $T_{\text{N}2}$, the spectrum indicates that there are two sizes of atomic magnetic moment, $0.357\mu_{\text{B}}$ and $0.216\mu_{\text{B}}$ at 4.2 K. There is no signal corresponding to null magnetic moment here, too.

(c) The integrated intensities of the two signals corresponding to these two sizes of moment are approximately equal to each other.

On the basis of these results, one can test the four cases as follows:

We first eliminate the Case 2 because on this model the neutron-diffraction result of the single-crystalline sample leads to a null atomic moment of some cerium atoms which is made by the superposition of \mathbf{q}_1^+ and \mathbf{q}_1^- modulations. The Case 3 also is eliminated because of a reason as will be mentioned later in conjunction with the results of the neutron diffraction under pressure. Then we discuss the Case 1 and the Case 4.

In the Case 1, the amplitude of each modulation is as given in Table I. The value of μ_2 in the table is calculated for the magnetic structure shown in Fig. 3, where the value of ϕ_2 is chosen to be $\pi/4$ so that all the Ce atoms have the same partial magnetic moment. If one superposes these three partial modulations as shown in Fig. 3 with the respective partial moments in Table I, one obtains three sizes of magnetic moment, that is, $0.47\mu_{\text{B}}$, $0.95\mu_{\text{B}}$, and $2.37\mu_{\text{B}}$. This is inconsistent with the NMR result (b), where only two sizes of moment are indicated.

On the other hand, if one choose $\phi_1=0$ and $\phi_2=\pi/2$ when superposing the three modulations, one obtains a structure as shown in Fig. 4, where the moments at the corners of the unit cell originate from the coupled \mathbf{q}_1^+ and \mathbf{q}_1^- modulations while so do at the body centers from the \mathbf{q}_2 modulation. In this case the magnitudes of the moments at the corners and the centers are calculated to be $1.42\mu_{\text{B}}$ and $1.34\mu_{\text{B}}$, respectively, and hence agree with each other within the experimental error. One may consider that this structure is most

acceptable because of its simple appearance. Moreover, it should be remarked that the spin configuration of this 4- \mathbf{q} structure maintains the tetragonal symmetry of the crystal lattice. We note that no evidence of crystal distortion toward orthorhombic lattice was observed, within the experimental error, in the nuclear reflections below $T_{\text{N}2}$.

One should note that the NMR results indicate two sizes of cerium moments, that is, $0.357\mu_{\text{B}}$ and $0.216\mu_{\text{B}}$, while the present 4- \mathbf{q} model predicts no significant difference between the moments of different sites. This inconsistency is explained in terms of the dissimilarity in the spin configurations of the cerium atoms around the silicon atoms. In Fig. 4, the crystal structure is such that a silicon atom is located at about $c/3$ away from a cerium atom along the c axis. Then, as far as the first-neighbor cerium atom concerns, all the silicon atoms are equivalent and should have the same magnitudes of the transferred hyperfine fields, though half of them have an opposite sign to the other half. However, if one assumes that the second-neighbor cerium atom along the c axis, which is located $\sim 2c/3$ away, is also effective to give a hyperfine field to the silicon, then the silicon atoms on the c axis connecting the corners of the b.c.t. unit cell (see Fig. 4) are no longer equivalent to those on the c axis connecting the body centers: For the former silicon, the first and the second cerium atoms have moments with the same signs, while opposite signs for the latter. Then, one may expect that the silicon atoms on these two nonequivalent sites should have different hyperfine fields from each other. The observed difference in the moments, hence in the hyperfine fields, can be explained if the silicon atom is supposed to be receiving hyperfine field from the second neighbor cerium atom which is $1/4$ as large as that from the first-neighbor cerium atom. It is, however, a matter of further argument if it is possible that a cerium atom at a distance from a silicon atom gives the same order of hyperfine field as one at the half distance does.

Case 4: In this case, if one assumes the same volumes for the \mathbf{q}_1 (\mathbf{q}_1^+ and \mathbf{q}_1^-) domain and the \mathbf{q}_2 domain as is indicated by the NMR, (c), one obtains $1.42\mu_{\text{B}}$ and $1.34\mu_{\text{B}}$ as the magnitudes of the moments in the respective phases, again in contradiction to the NMR result.

Before considering more on the 4- \mathbf{q} state and the multi-domain state, we show a part of the results of the high-pressure diffraction experiments. In Fig. 5 shown are the intensities of the reflections under several magnitudes of the applied pressure. In the figure, one can see that, under pressure of 0.18 GPa, the \mathbf{q}_1^- reflection has lost most of its intensity in the temperature region $T_{\text{N}2} < T < T_{\text{N}1}$ and that the \mathbf{q}_1^+ reflection is, instead, approximately twice as intense as that under the ambient pressure. Obviously this phenomenon should be attributed to the effect of the possible remanent uniaxial component of the pressure which the piston-cylinder type pressure cell is often subject to. Because the cylinder axis is parallel to \mathbf{q}_1^- (see Fig. 2), the compressive stress along the wave vector must have suppressed the growing of the \mathbf{q}_1^- domains. This observation is a proof that the \mathbf{q}_1^+ and the \mathbf{q}_1^- phases form independent domains in this temperature region. The most remarkable feature in this figure is the behavior of the intensity of the \mathbf{q}_1^- reflection when temperature is decreased below $T_{\text{N}2}$: The intensity of the \mathbf{q}_2 reflection starts growing at $T_{\text{N}2}$, then simultaneously the \mathbf{q}_1^- reflection

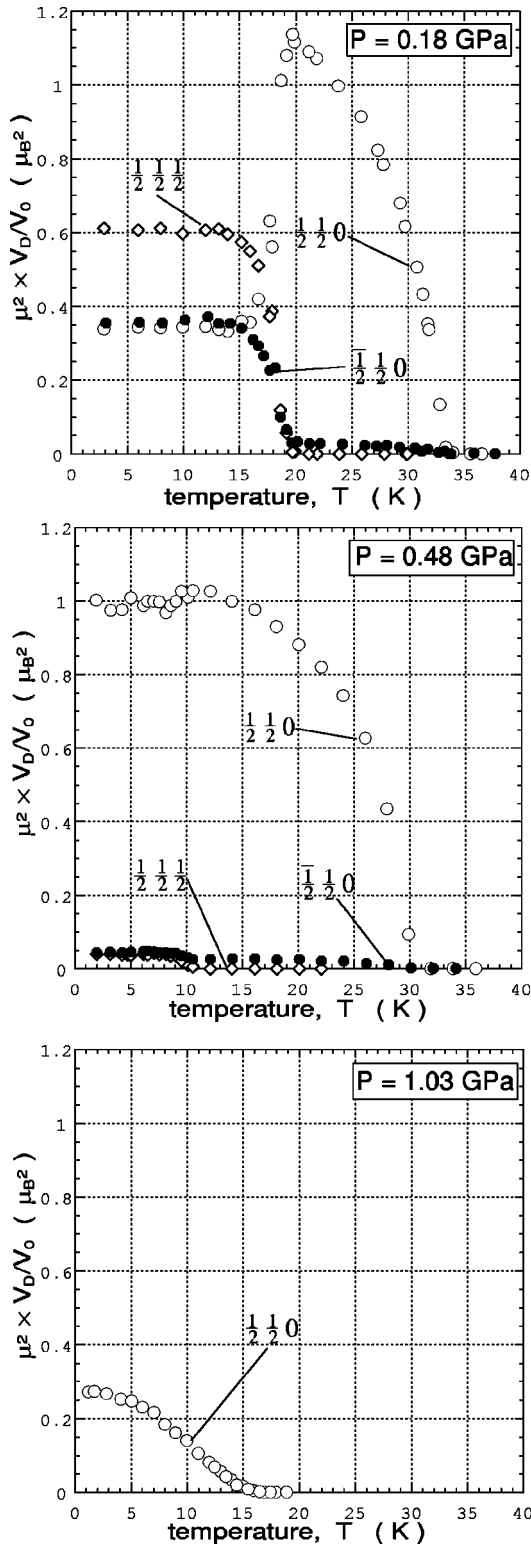


FIG. 5. The temperature dependences of the scattering intensities from the single-crystalline CeRh_2Si_2 under pressure of 0.18, 0.48, and 1.03 GPa. The unit of the ordinate is the same as the one in Fig. 1.

revives and start growing to reach the same intensity, at the lowest temperature, as that of the \mathbf{q}_1^+ reflection. All these behaviors of all the reflections have, as was the case at the ambient pressure, good reproducibility with respect to repeated thermal cycles, and hence the system seems to be in

thermal equilibrium at any temperature. One should remind that in an ordinary antiferromagnet the domains are randomly distributed as a result of the random nucleation-and-growth and any external perturbation which prefers one type of domain to the others can help the particular domain to dominate over the crystal. Thus, a multidomain structure is subject to thermal hysteresis effect under such perturbations. We, therefore, consider that the present observation is a good evidence for the $4\text{-}\mathbf{q}$ ground structure in CeRh_2Si_2 . This behavior of the \mathbf{q}_1^- reflection eliminates the possibility of the Case 3 in the previous argument: In this case, the phases $(\mathbf{q}_1^+ + \mathbf{q}_2)$ and $(\mathbf{q}_1^- + \mathbf{q}_2)$ must degenerate and reside in different domains from each other. It is not likely to happen that the \mathbf{q}_1^- modulation is restored to help $(\mathbf{q}_1^- + \mathbf{q}_2)$ phase to survive the uniaxial stress which disfavors it.

The remaining problem on the ground-state magnetic structure of CeRh_2Si_2 is the inconsistency in the size of the ordered moment: We obtained the value $1.38\mu_B/\text{Ce}$ (the average of $1.42\mu_B$ and $1.34\mu_B$) from the present study, while the NMR study⁸ predicts $0.357\mu_B$ and $0.216\mu_B/\text{Ce}$. These values do not depend on the model structure, $4\text{-}\mathbf{q}$ or multidomain, and the discrepancy in them is significantly larger than the experimental errors in both studies. Since in the case of CePd_2Si_2 the NMR results indicated a value of the magnetic moment which is in reasonable agreement with the neutron diffraction result, the present conflict seems to be caused by an intrinsic nature of the magnetism of CeRh_2Si_2 . There may be, as has been previously discussed,⁸ a longitudinal fluctuation of the f -electron moment which has a lifetime longer than the characteristic time of observation for thermal neutrons but shorter than that for NMR. A question to this argument, however, arises from the fact that the transition temperatures T_{N1} and T_{N2} have no significant difference in between both experiments: It is expected that such a fluctuation should give a lower transition temperature to the observation by the NMR than to the one by the neutron diffraction. A μSR experiment, which has the same order of the time of the observation as the NMR, will provide a helpful information on this problem.

B. Response to high pressure

The hydrostatic pressure was applied up to 1.25 GPa, and the results of the intensity measurements of the magnetic reflections under 0.48 and 1.03 GPa are shown as examples also in Fig. 5. In the figure, one can see that the intensities of the \mathbf{q}_1^- and \mathbf{q}_2 reflections under the pressure of 0.48 GPa have been remarkably suppressed. It is, however, noticeable that the intensity ratio of the \mathbf{q}_2 reflection to the \mathbf{q}_1^- reflection retains the value of approximately 2. This indicates that the $4\text{-}\mathbf{q}$ phase coexists with the \mathbf{q}_1^+ phase though with very small volume. The $4\text{-}\mathbf{q}$ phase was not observed at all under the pressure of 0.79 GPa. The T_{N1} and the T_{N2} , here the T_{N2} is defined as the onset temperature of the $4\text{-}\mathbf{q}$ phase, are plotted in Fig. 6 as functions of the applied pressure. In the figure, one can see that both of the T_{N1} and the T_{N2} decrease with increasing pressure and the system becomes nonmagnetic under pressure greater than the critical magnitude of $P_c = 1.1$ GPa and also that the change of the T_{N1} is very steep around P_c . This feature of the two transition temperatures is quite consistent with the results of the resistivity measure-

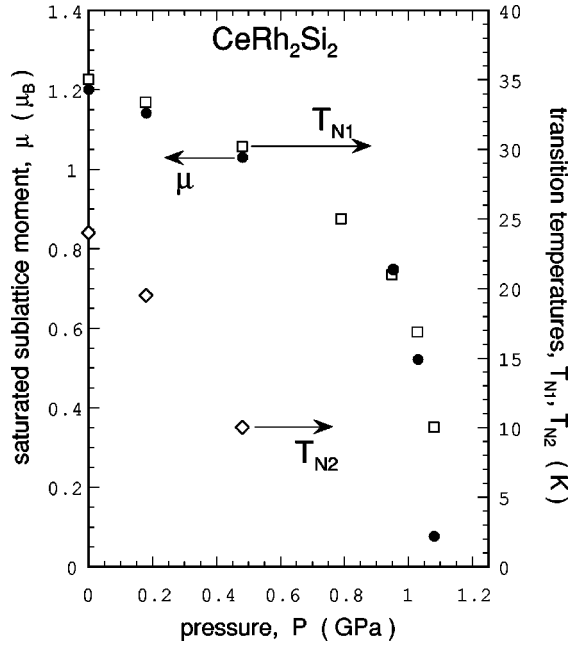


FIG. 6. The saturated sublattice moment (per cerium atom) and the transition temperatures as functions of the applied pressure. At $P=0.79$ GPa, we failed to determine the magnitude of the moment in the absolute scale but obtained only the transition temperature.

ments by Grosche *et al.*¹⁶ and Thompson *et al.*¹⁷ In Fig. 6 also is shown the magnitude of the saturated ordered magnetic moment, μ , as a function of the pressure. In the figure, one should note that the saturated ordered moment starts decreasing immediately when the pressure is applied in the same way as T_{N1} does. In order to make this point clear, we plot in Fig. 7 the magnitude of the saturated ordered moment as a function of the transition temperature by taking the pressure as the implicit parameter. In the figure, it is remarkable that the magnitude of the ordered moment is proportional to the transition temperature up to 1.03 GPa. This means that the atomic magnetic moment of cerium in this compound is variable longitudinally, which is rather unexpected from its extraordinary high Néel temperature: If the cerium atom has a well-defined localized moment, the ordered moment in Fig. 7 should be independent of the transition temperature at least in the region of small pressure. The proportionality between the ordered moment and the transition temperature is characteristic of the itinerant electron magnets and has been typically observed in the spin-density wave phase of the chromium alloys.¹⁸ We therefore conclude that the character of the magnetic order in CeRh_2Si_2 is metallic from the view point of the longitudinal flexibility of the atomic magnetic moment. Another important feature in Fig. 7 is that the point for 1.08 GPa deviates significantly from the linear relation. The sublattice moment at this pressure saturates at $0.076\mu_B/\text{Ce}$ and depends on temperature quite normally with a clearly defined transition temperature $T_N=10.0$ K as shown in the inserted figure. If one extrapolates the curve connecting all the points in Fig. 7, it seems that the curve approaches the T_N coordinate at a nonzero value of T_N around 10 K. As a matter of course, it makes no sense to expect that the system with an absolutely null ordered moment has a finite transition temperature. However, one can reasonably expect from Fig. 7 that, if the pressure is properly increased

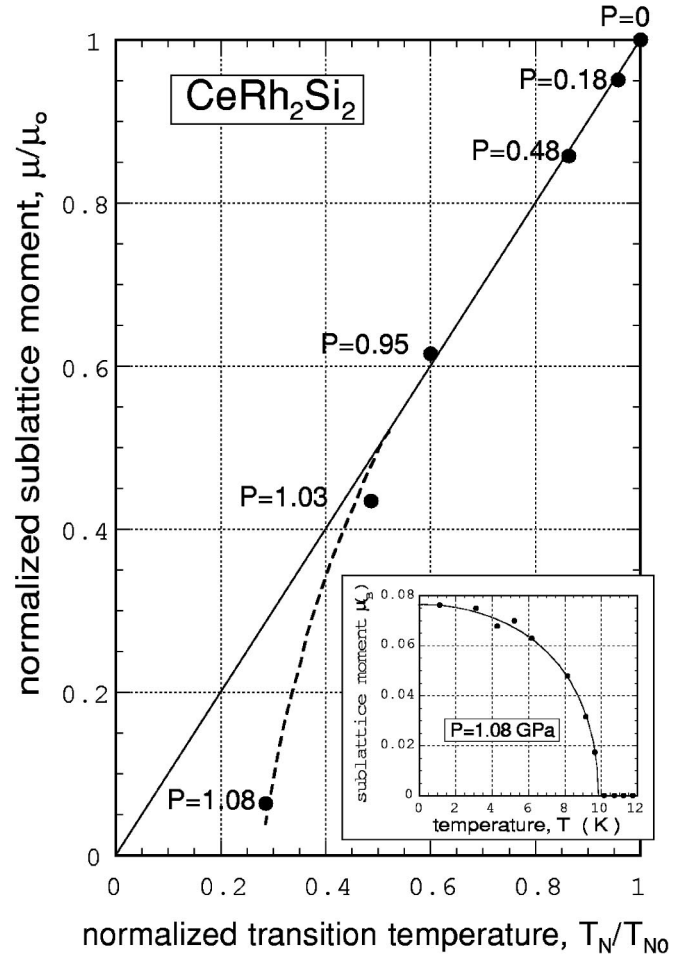


FIG. 7. The saturated sublattice moment (per cerium atom) as a function of the transition temperature T_{N1} . The moment and the transition temperature are normalized at the ambient pressure. The broken line is a guide to eyes. The unit of the pressure is GPa. The inset figure shows the temperature dependence of the sublattice moment at $P=1.08$ GPa.

a little more, the system must have a moment much smaller than $0.076\mu_B/\text{Ce}$ with no significant shift in T_N from 10 K. The figure indicates that the system undergoes, with increasing pressure, two different electronic states one after the other: One is characterized by the proportionality of the μ and the T_N (this state is denoted as the low-pressure state), and so is the other (denoted as the critical-pressure state) by the moment which reduces toward zero at the nonzero transition temperature.

Contraction of a Kondo-lattice crystal due to pressure causes increase of the Kondo temperature through the increase of the hybridization of the f electrons and the conduction electrons. When temperature is reduced much lower than the Kondo temperature, a hybridization gap (the coherence gap) is formed by the Fermi level and its size takes place of the hybridization energy $k_B T_K$ as the energy scale of the system.¹⁹ The Kondo temperature of CeRh_2Si_2 has been estimated to be about 100 K from the observed behavior of $1/T_1$ of NMR,⁸ though not established. Because, as has already been discussed, the magnetism of CeRh_2Si_2 is metallic at the ambient pressure the Kondo temperature is expected to be at least comparable with or higher than its Néel temperature of 35 K, being consistent with the NMR result. We,

therefore, consider that, under the pressure of 1.08 GPa, the coherence of the coupled f electron and the conduction electron must have been fully developed at 10 K. Then, we regard that the critical-pressure state of CeRh₂Si₂ is the well-grown coherent state with a tiny-moment order in. One may speculate, by generalizing the present observation, that the tiny-moment ordering is a rather common nature of the ground coherent state of metallic heavy fermion compounds

where the Ruderman-Kittel-Kasuya-Yosida interaction and the Kondo effect are marginally competing with each other.

It was very difficult to make fine-tuning of pressure at P_c . Indeed, we achieved the pressure of 1.08 GPa quite incidentally. We believe, however, that more detailed study around P_c of CeRh₂Si₂ will provide rich information to understand the origin of the tiny-moment ordering in the heavy-fermion compounds.

-
- ¹B. H. Grier, J. M. Lawrence, V. Murgai, and R. D. Parks, Phys. Rev. B **29**, 2664 (1984).
- ²S. Kawarazaki, Y. Kobashi, J. A. Fernandez-Baca, S. Murayama, Y. Onuki, and Y. Miyako, Physica B **206&207**, 298 (1995).
- ³R. Settai, A. Misawa, S. Araki, M. Kosaki, K. Sugiyama, T. Takeuchi, K. Kindo, H. Haga, E. Yamamoto, and Y. Onuki, J. Phys. Soc. Jpn. **66**, 2260 (1997).
- ⁴S. Araki, A. Misawa, R. Settai, T. Takeuchi, and Y. Onuki, J. Phys. Soc. Jpn. **67**, 2915 (1998).
- ⁵R. Movshovich, T. Graf, D. Mandrus, J. D. Thompson, J. L. Smith, and Z. Fisk, Phys. Rev. B **53**, 8241 (1996).
- ⁶R. Movshovich, T. Graf, D. Mandrus, M. F. Hundley, J. D. Thompson, R. A. Fisher, N. E. Phillips, and J. L. Smith, Physica B **223&224**, 126 (1996).
- ⁷S. Kawarazaki, K. Fujita, K. Yasuda, Y. Sasaki, T. Mizusaki, and A. Hirai, Phys. Rev. Lett. **61**, 471 (1988).
- ⁸Y. Kawasaki, K. Ishida, Y. Kitaoka, and K. Asayama, Phys. Rev. B **58**, 8634 (1998).
- ⁹G. Aeppli, E. Bucher, C. Broholm, J. K. Kjems, J. Baumann, and J. Hufnagl, Phys. Rev. Lett. **60**, 615 (1988).
- ¹⁰C. Broholm, J. K. Kjems, W. J. L. Buyers, P. Matthews, T. T. M. Palstra, A. A. Menovsky, and J. A. Mydosh, Phys. Rev. Lett. **58**, 1467 (1987).
- ¹¹A. Amato, C. Bains, R. Feyerherm, J. Flouquet, F. N. Gygax, P. Lejay, A. Schenk, and U. Zimmermann, Physica B **186-188**, 276 (1993).
- ¹²A. Onodera, Y. Nakai, N. Kunitomi, O. A. Pringle, H. Smith, R. Nicklow, R. Moon, F. Amita, N. Yamamoto, S. Kawano, N. Achiwa, and Y. Endoh, Jpn. J. Appl. Phys., Part 1 **26**, 152 (1987).
- ¹³G. H. Lander and T. O. Brun, J. Chem. Phys. **53**, 1387 (1970).
- ¹⁴A. J. Freeman and J. P. Desclaux, J. Magn. Magn. Mater. **12**, 11 (1979).
- ¹⁵Y. A. Izyumov, V. E. Naish, and R. P. Ozerov, *Neutron Diffraction of Magnetic Materials* (Plenum, New York, 1991).
- ¹⁶F. M. Grosche, S. R. Julian, N. D. Mathur, F. V. Carter, and G. G. Lonzarich, Physica B **237-238**, 197 (1997).
- ¹⁷J. D. Thompson, R. D. Parks, and H. Borges, J. Magn. Magn. Mater. **54-57**, 377 (1986).
- ¹⁸E. Fawcett, H. L. Alberts, V. Yu. Galkin, D. R. Noakes, and J. V. Yakhmi, Rev. Mod. Phys. **66**, 25 (1994).
- ¹⁹C. Lacroix, J. Magn. Magn. Mater. **63&64**, 239 (1987).